






# Native and activated antithrombin inhibits TMPRSS2 activity and SARS-CoV-2 infection

Lukas Wettstein<sup>1</sup>  | Patrick Immenschuh<sup>1</sup>  | Tatjana Weil<sup>1</sup>  |  
Carina Conzelmann<sup>1</sup>  | Yasser Almeida-Hernández<sup>2</sup>  | Markus Hoffmann<sup>3,4</sup> |  
Amy Kempf<sup>3,4</sup> | Inga Nehlmeier<sup>3</sup> | Rishikesh Lotke<sup>5</sup> | Moritz Petersen<sup>5</sup> |  
Steffen Stenger<sup>6</sup> | Frank Kirchhoff<sup>1</sup> | Daniel Sauter<sup>5</sup> | Stefan Pöhlmann<sup>3,4</sup> |  
Elsa Sanchez-Garcia<sup>2</sup> | Jan Münch<sup>1</sup>

<sup>1</sup>Institute of Molecular Virology, Ulm University Medical Center, Ulm, Germany

<sup>2</sup>Computational Biochemistry, Center of Medical Biotechnology, University of Duisburg-Essen, Essen, Germany

<sup>3</sup>Infection Biology Unit, German Primate Center-Leibniz Institute for Primate Research, Göttingen, Germany

<sup>4</sup>Faculty of Biology and Psychology, Georg-August-University, Göttingen, Germany

<sup>5</sup>Institute for Medical Virology and Epidemiology of Viral Diseases, University Hospital Tübingen, Tübingen, Germany

<sup>6</sup>Institute for Microbiology and Hygiene, Ulm University Medical Center, Ulm, Germany

## Correspondence

Jan Münch, Institute of Molecular Virology,  
Ulm University Medical Center, Ulm 89081,  
Germany.

Email: [jan.muench@uni-ulm.de](mailto:jan.muench@uni-ulm.de)

## Funding information

German Research Foundation (DFG) through  
"Fokus-Förderung COVID-19" (FR 2974/3-1,  
KL 2544/8-1); Deutsches Zentrum für  
Infektionsforschung; BMBF (01KI20135);  
Major instrumentation granted under the  
DFG- Projektnummer: 436586093; BMBF  
(RAPID Consortium, 01KI1723D and  
01KI2006D; RENACO, 01KI20328A,  
01KI20396; DFG within the CRC 1279  
"Exploiting the Human Peptidome for Novel  
Antimicrobial and Anticancer Agents";  
DFG under Germany's Federal and State  
Excellence Strategy EXC- 2033 Projektnummer  
390677874; EU's Horizon 2020 research and  
innovation programme (Fight-nCoV,  
101003555 to J. M.); Sonderfördermassnahme  
COVID-19 of the MWK Baden-Württemberg,  
Germany; DFG Heisenberg Programme,  
Grant/Award Number: SA2676/3-1

## Abstract

Host cell proteases such as TMPRSS2 are critical determinants of severe acute respiratory syndrome coronavirus 2 (SARS-CoV-2) tropism and pathogenesis. Here, we show that antithrombin (AT), an endogenous serine protease inhibitor regulating coagulation, is a broad-spectrum inhibitor of coronavirus infection. Molecular docking and enzyme activity assays demonstrate that AT binds and inhibits TMPRSS2, a serine protease that primes the Spike proteins of coronaviruses for subsequent fusion. Consequently, AT blocks entry driven by the Spikes of SARS-CoV, MERS-CoV, hCoV-229E, SARS-CoV-2 and its variants of concern including Omicron, and suppresses lung cell infection with genuine SARS-CoV-2. Thus, AT is an endogenous inhibitor of SARS-CoV-2 that may be involved in COVID-19 pathogenesis. We further demonstrate that activation of AT by anticoagulants, such as heparin or fondaparinux, increases the anti-TMPRSS2 and anti-SARS-CoV-2 activity of AT, suggesting that repurposing of native and activated AT for COVID-19 treatment should be explored.

## KEYWORDS

antithrombin, protease inhibitor, SARS-CoV-2, SERPINC1, TMPRSS2

Lukas Wettstein and Patrick Immenschuh contributed equally to this study.

This is an open access article under the terms of the Creative Commons Attribution-NonCommercial-NoDerivs License, which permits use and distribution in any medium, provided the original work is properly cited, the use is non-commercial and no modifications or adaptations are made.

© 2022 The Authors. *Journal of Medical Virology* published by Wiley Periodicals LLC.

## 1 | INTRODUCTION

The emergence and pandemic spread of the severe acute respiratory syndrome coronavirus 2 (SARS-CoV-2) poses a major global health crisis. Even though protective vaccines are available, there is still an urgent need for the development of specific antivirals to prevent SARS-CoV-2 spread into the lung or treat COVID-19.<sup>1</sup> SARS-CoV-2 infection is mediated by the viral Spike (S) glycoprotein, which comprises two subunits, S1 and S2.<sup>2,3</sup> The S1 subunit harbors the receptor binding domain (RBD) and binds to the cellular receptor ACE2, while the S2 subunit anchors the S protein in the viral membrane and harbors determinants required for virus-cell fusion. Following engagement of ACE2, proteolytic cleavage of the S2 subunit occurs by the cellular proteases transmembrane serine protease serine subtype 2 (TMPRSS2), cathepsins B or L or furin at the so-called S2' site.<sup>4,5</sup> Cleavage is thought to prime the S protein for membrane fusion by triggering conformational changes allowing viral entry.<sup>3,5,6</sup> Inhibitors of TMPRSS2 enzymatic activity such as camostat or nafamostat prevent S protein priming and consequently viral infection,<sup>5,7-11</sup> and are currently in the clinical evaluation as COVID-19 therapeutics.

Previous reports show that the serine protease inhibitor (serpin)  $\alpha_1$ -antitrypsin ( $\alpha_1$ AT, SERPINA1) is an endogenous inhibitor of TMPRSS2 activity and SARS-CoV-2 entry, with potential application for COVID-19 treatment.<sup>12,13</sup> Until today, 36 human serpins have been identified and linked to the regulation of physiological processes such as hemostasis, immunity, and inflammation.<sup>14,15</sup> However, it remains largely unclear which serpins can interfere with SARS-CoV-2 infection. The serpin antithrombin (SERPINC1) is a serum protein with a physiological concentration of ~0.15 mg/ml, equivalent to ~2.6  $\mu$ M.<sup>16</sup> Its main function is the regulation of coagulation through inhibition of serine proteases including factor IXa, Xa, and thrombin. However, it also displays affinity to other proteases such as trypsin, papain, and cathepsin L.<sup>17-20</sup> The target protease recognizes and cleaves a distinct region of antithrombin (AT), the so-called reactive center loop (RCL). The subsequent formation of a covalently bound acyl-enzyme intermediate between serpin and protease triggers conformational changes in the serpin, which physically disrupts the protease reactive center and result in an irreversible inhibition.<sup>21,22</sup> Herein, we investigated whether AT inhibits TMPRSS2 and consequently SARS-CoV-2 infection.

## 2 | MATERIALS AND METHODS

### 2.1 | Computational modeling

For modeling the TMPRSS2-AT interaction, a TMPRSS2 homology model deposited in the SwissModel repository<sup>23</sup> (UniProtKB ID: O15393) was superimposed onto the crystal structure of the factor IXa-AT-pentasaccharide complex (PDB ID: 3KCG).<sup>24</sup> The initial docking model was refined with HADDOCK,<sup>25</sup> GalaxyRefineComplex,<sup>26,27</sup> and Rosetta.<sup>28</sup> The 10 best-scored solutions from each tool were selected and applied to Rosetta's<sup>28</sup> high-resolution refinement protocol. The best-scored solution was refined in the presence of

explicit solvent and the system was neutralized with NaCl. To this end, NPT unrestrained simulated annealing MD simulations were performed (2 replicas) with the CHARMM36 force field<sup>29</sup> and the GROMACS simulation package.<sup>30</sup> The initial reference temperature was 300 K and the system was subjected to three 10 ns cycles of heating to 320 K and stepwise cooling to 275 K.

### 2.2 | Reagents

Camostat mesylate (CM) (SML0057) and E64-d (E8640) were obtained from Merck. AT was obtained from CSL Behring (Kybernin<sup>®</sup>) and Grifols (Anbinex<sup>®</sup>) and solubilized in ddH<sub>2</sub>O. Fondaparinux (SML1240) and heparin (H3149) were obtained from Merck, Boc-Gln-Ala-Arg-AMC peptide was obtained from Bachem (40170 19.0005), EK1 peptide (H2N-SLDQINVTFLDLEYEMKKLEEAIAKLEE SYIDLKEL-COOH) was synthesized in-house by solid phase synthesis. Recombinant TMPRSS2 was obtained from CreativeBiomart (TMPRSS2-1856H) or LSBio (LS-G57269).

### 2.3 | BCA assay

Protein concentration in the reconstituted AT preparations Anbinex and Kybernin was determined with a commercially available bicinchoninic acid (BCA) assay kit (Pierce<sup>™</sup> BCA Protein Assay Kit; Thermo Fisher Scientific) using a VERSAMax microplate reader with SoftMax Pro 7.0.3 software.

### 2.4 | Filtration and gel electrophoresis

AT preparations were subjected to a 10 kDa centrifugal filter (Amicon Ultra-0.5 ml Ultracel-10k) at 14,000g. Retentate and flowthrough were collected and adjusted to match the input volume. One microgram of protein per sample was then applied to reduce sodium dodecyl sulfate polyacrylamide gel electrophoresis on a 4%-12% Bis-Tris protein gel (NuPAGE<sup>™</sup>) with MES running buffer. Before electrophoresis, samples were reduced with 50 mM TCEP and heated for 10 min at 70°C. The gel was stained with Coomassie G-250 (GelCode<sup>™</sup> Blue Stain).

### 2.5 | Activation of AT

For the activation of AT, serial dilutions of heparin or FPX were mixed with constant concentrations of AT and incubated for 1 h at 37°C before use.

### 2.6 | TMPRSS2 activity assay

For analysis of purified TMPRSS2, serially diluted AT, activated AT, CM, or E64-d were mixed with 25  $\mu$ l of 2  $\mu$ g/ml recombinant

TMPRSS2 in assay buffer (50 mM Tris-HCl, 0.154 mM NaCl pH 8.0) for 10 min at 37°C, followed by addition of 50 µl of 20 µM BOC-QAR-AMC protease substrate. Fluorescence intensity was recorded at an excitation wavelength of 380 nm and emission wavelength of 460 nm immediately after addition of substrate and after 3 h at 37°C in a TECAN Genios microplate reader with Magellan V6.4 software or in a Synergy™ H1 microplate reader (BioTek) with Gen 5 3.04 software.

To assess the activity of cellular TMPRSS2, 20 000 HEK293T cells were seeded in respective growth medium in a 96-well flat bottom plate. The next day, cells were transfected with 100 ng of TMPRSS2 expression plasmid (addgene 53887, kindly provided by Prof. Roger Reeves, Johns Hopkins University, Baltimore, United States) per well using polyethyleneimine (PEI) transfection reagent. Briefly, plasmid DNA was mixed with PEI in a 3:1 ratio in serum-free medium, incubated for 20 min at RT, and added to cells dropwise. At 16 h post-transfection, the medium was removed and 60 µl of serum-free medium was added followed by addition of serial dilutions of AT preparations, activated AT or CM. After incubation for 15 min at 37°C, 20 µl of 500 µM protease substrate (BOC-QAR-AMC) were added. Fluorescence intensity was recorded at an excitation wavelength of 380 nm and emission wavelength of 460 nm immediately after addition of substrate and after 2 h at 37°C in a Synergy™ H1 microplate reader (BioTek) with Gen 5 3.04 software.

## 2.7 | Cathepsin activity assay

Serial dilutions of AT, CM, or E64-d were mixed with recombinant cathepsin L (R & D, 952-Cy) in assay buffer (50 mM MES, 5 mM DTT, 1 mM ethylenediamine tetraacetic acid [EDTA], 0.005% Brij35, pH 6) or with cathepsin B from human placenta (Sigma Aldrich; C0150) in assay buffer (105.6 mM KH<sub>2</sub>PO<sub>4</sub>, 14.4 mM Na<sub>2</sub>HPO<sub>4</sub>, 1.2 mM EDTA, 0.07% Brij35, 2.4 mM L-cysteine, pH 6). The protease-inhibitor mixtures were incubated for 10 min at RT, before adding fluorogenic reporter substrate Z-Leu-Arg-AMC (for cathepsin L) or Z-Arg-Arg-AMC (for cathepsin B). Final concentrations were as follows: cathepsin L 0.01 µg/ml, cathepsin B 1 µg/ml, Z-Leu-Arg-AMC 40 µM or Z-Arg-Arg-AMC 30 µM. Fluorescence intensity was recorded at an excitation wavelength of 380 nm and emission wavelength of 460 nm after 25 min at 37°C (cathepsin L) or after 60 min at 40°C (cathepsin B) in a Synergy™ H1 microplate reader (BioTek) with Gen 5 3.04 software.

## 2.8 | Furin activity assay

Serial dilutions of AT were mixed with recombinant furin (R & D; 1503-SE-010) in assay buffer (25 mM Tris, 1 mM CaCl<sub>2</sub>, pH 9) for 10 min at 37°C, followed by addition of 50 µl of 20 µM succinyl (Suc.) modified QTNSPRRAR-AMC protease substrate. The final concentration of furin was 1.5 ng/µl. Fluorescence intensity was recorded at 2-min intervals for 5 h at an excitation wavelength of 355 nm and

emission wavelength of 460 nm at 37°C in a Cytation 3 (BioTek) microplate reader. The area under the curve values normalized to furin control was plotted. The activity of activated AT on furin was assessed as described above, using activated AT.

## 2.9 | Cell culture

Unless stated otherwise, HEK293T cells (ATCC, CRL-3216) were cultivated in dulbecco's modified eagle medium (DMEM) supplemented with 10% fetal calf serum (FCS), 2 mM L-glutamine, 100 U/ml penicillin and 100 µg/ml streptomycin. Caco2 cells (kindly provided by Prof. Holger Barth, Ulm University, Ulm, Germany; ATCC, HTB-37) were cultivated in DMEM supplemented with 10% FCS, 2 mM glutamine, 100 U/ml penicillin, and 100 µg/ml streptomycin, 1× non-essential amino acids (NEAA) and 1 mM sodium pyruvate. Vero E6 cells (ATCC, CRL-1586) were cultivated in DMEM supplemented with 2.5% (FCS), 2 mM L-glutamine, 100 U/ml penicillin, 100 µg/ml streptomycin, 1× NEAA and 1 mM sodium pyruvate. Calu-3 cells (ATCC, HTB-55) were cultivated in MEM supplemented with 10% FCS, 100 U/ml penicillin and 100 µg/ml streptomycin, 1× NEAA and 1 mM sodium pyruvate.

## 2.10 | Cytotoxicity assay

To assess the cytotoxicity of AT preparations, heparin, Fondaparinux (FPX), and CM, 10,000 Caco2 cells were seeded in respective growth medium in a 96-well flat bottom plate. The next day, the medium was replaced by 80 µl of serum-free medium, and cells were treated with serial dilutions of AT, heparin, FPX, CM, or Phosphate-buffered saline (PBS) as control. After 16 h, cell viability was assessed by measuring ATP levels in cell lysates with a commercially available kit (CellTiter-Glo®, Promega) in an Orion II microplate reader with simplicity 4.2 software. The signal from PBS-treated cells served as a control and was used for normalization.

## 2.11 | Rhabdoviral pseudoparticles

For the generation of VSV-based SARS-CoV-2 Spike (VSV (Luc\_eGFP)-CoV-2-S) and VSV glycoprotein pseudoparticles (VSV (Luc\_eGFP)-G), 10,000,000 HEK293T cells were seeded in respective growth medium in a T175 cell culture flask. The next day, cells were transfected with a total of 44 µg glycoprotein expression plasmid using Transit-LT-1 (Mirus). Plasmid DNA and LT-1 were mixed in 4 ml of OptiMEM at a 1:3 ratio, incubated for 20 min at RT, and added to cells dropwise. 24 h post-transfection, the medium was replaced and cells were transduced with VSV-G pseudotyped VSV encoding a luciferase and a green fluorescent protein reporter gene (kindly provided by Gert Zimmer, Institute of Virology and Immunology, Mittelhäusern, Switzerland<sup>31</sup>). At 3 h post-transduction, cells were washed three times with PBS and cultivated for 16 h in HEPES buffered HEK293T medium. Virus-containing supernatants were

then harvested and clarified by centrifugation for 5 min at 2000g. Residual pseudoparticles harboring VSV-glycoprotein were blocked by addition of anti-VSV-G hybridoma supernatant at 1:10 volume ratio (I1, mouse hybridoma supernatant from CRL-2700; ATCC). Virus stocks were aliquoted and stored at  $-80^{\circ}\text{C}$  until use.

## 2.12 | Lentiviral pseudoparticles

For the generation of lentiviral SARS-CoV-2 Spike (LV(Luc)-CoV-2-S) pseudoparticles, 900 000 HEK293T cells were seeded in respective growth mediums in a six-well plate. The next day cells were transfected with 0.49  $\mu\text{g}$  of pCMVdr8\_91 (encoding a replication-deficient lentivirus), 0.49  $\mu\text{g}$  of pSEW-Luc2 (encoding a luciferase reporter gene, both kindly provided by Prof. Christian Buchholz, Paul-Ehrlich-Institute, Germany), and 0.02  $\mu\text{g}$  of either pCG1-SARS-2-S $\Delta$ 18 (WT), pCG1-SARS-2-S $\Delta$ 18 (B.1.1.7, Alpha), pCG1-SARS-2-S $\Delta$ 18 (B.1.351, Beta), pCG1-SARS-2-S $\Delta$ 18 (B.1.1.28, P1, Gamma), pcDNA3\_1 SARS-CoV-2-S d19 B.1.617.2\_4377 (B.1.617.2, Delta), or pCG1\_SARS-2-S $\Delta$ 18 (B.1.1.529, Omicron) by mixing the plasmid DNA with PEI at a 1:3 ratio in serum-free medium. After 20 min incubation at RT, transfection mix was added to cells dropwise. The cells were washed 8 h posttransfection and a growth medium containing 2.5% FCS was added. At 48 h post-transfection, pseudoparticle containing supernatants were harvested and clarified by centrifugation for 5 min at 450g. Virus stocks were aliquoted and stored at  $-80^{\circ}\text{C}$  until use.

## 2.13 | Transduction of Caco2 cells

One day before transduction, 10 000 Caco2 cells were seeded in respective growth medium in a 96-well flat bottom plate. The next day medium was replaced by 60  $\mu\text{l}$  serum-free growth medium and cells were treated with AT, filtered AT, CM, or EK1 for indicated times at  $37^{\circ}\text{C}$  followed by transduction of cells with 20  $\mu\text{l}$  of rhabdoviral or lentiviral pseudoparticles. To investigate AT treatment of cells posttransduction, the medium was replaced by 80  $\mu\text{l}$  of the serum-free growth medium, and cells were transduced with 20  $\mu\text{l}$  of infectivity normalized pseudoparticles. At indicated time points, cells were washed with 100  $\mu\text{l}$  PBS and 80  $\mu\text{l}$  serum-free medium as well as 20  $\mu\text{l}$  of serially diluted AT were added. Transduction rates were assessed by measuring luciferase activity in cell lysates at 16 h (rhabdoviral pseudoparticles) or 48 h (lentiviral pseudoparticles) post-transduction with a commercially available kit (Luciferase Assay System; Promega) in an Orion II microplate reader with simplicity 4.2 software. Values for untreated controls were set to 100% transduction.

## 2.14 | SARS-CoV-2 strains and propagation

SARS-CoV-2 isolates BetaCoV/Netherlands/01/NL/2020 (#010V-03903) (Wuhan-Hu-1, Spike mutation D614G) and hCoV-19/Netherlands/NoordHolland\_20432/2020, VOC 202012/01, next

strain clade 20B (lineage B.1.1.7 or Alpha) were obtained from the European Virus Archive global. The SARS-CoV-2 isolate of lineage B.1.617.2 or Delta was kindly provided by Prof. Hendrik Streeck, Bonn University Medical Center, Bonn, Germany. The virus lineage B.1.617.2 (Delta) was isolated in Bonn from a throat swab of a patient on Caco2 cells cultured in DMEM medium (10% FCS, 100  $\mu\text{g}/\text{ml}$  streptomycin, 100 U/ml penicillin, and 2.5  $\mu\text{g}/\text{ml}$  amphotericin B). The nature of the Delta variant was determined by melting curve analyses of marker mutants (TIB MOLBIOL) and sequencing analyses of amino acids 420-719 of the Spike protein. The latter confirmed mutations L452R, T478K, D614G, and P681R. For propagation of SARS-CoV-2 strains, Caco2 cells were seeded to 70%–90% confluency in a T175 cell culture flask and inoculated with respective isolates at an multiplicity of infection (MOI) of 0.03–0.1 in 3.5 ml serum-free medium. After 2 h of incubation at  $37^{\circ}\text{C}$ , 20 ml of growth medium supplemented with 15 mM HEPES were added. Upon the occurrence of cytopathic effect (CPE), virus-containing supernatants were harvested and separated from cellular debris by centrifugation for 5 min at 1000g. Virus stocks were aliquoted and stored at  $-80^{\circ}\text{C}$  until use. Infectious virus titer was determined as plaque-forming units (PFU) on VeroE6 cells and used to calculate MOI by dividing the PFU by the number of cells (assuming a duplication of cell number between seeding and infection).

## 2.15 | Infection of Caco2 cells with SARS-CoV-2

Twenty-five thousand Caco2 cells were seeded in respective growth medium in a 96-well flat-bottom plate. The next day, cells were treated with serially diluted AT, activated AT, or CM for 1 h followed by infection either with SARS-CoV-2 WT (D614G) at an MOI of 0.0002 for 2 days or with SARS-CoV-2 WT (D614G), B.1.1.7, or B.1.617.2 at an MOI of 0.005 for 1 day. For analysis of infection rates, cells were detached and fixed in 4% PFA for 30 min, washed with PBS, and stained for flow cytometry using a commercially available buffer (Fix & Perm; MuBio Nordic). Briefly, cells were incubated with SARS-CoV-2 nucleocapsid antibody (Sino Biological, 40143-MM05) diluted 1:1000 in Buffer B for 30 min at  $4^{\circ}\text{C}$ . Cells were washed twice with FACS buffer (1% FCS in PBS), incubated with AlexaFluor488 labeled anti-mouse antibody (Thermo Fisher Scientific; A32723) diluted 1:400 in FACS buffer for 30 min at  $4^{\circ}\text{C}$ , and washed twice with FACS buffer. Analysis was performed using a CytoflexLX flow cytometer (Beckmann Coulter) with CytExpert 2.3 software. The signal from PBS-treated, infected cells served as control and was used for normalization. The gating strategy is depicted in Supporting Information: Figure 8.

## 2.16 | Infection of Calu-3 cells with SARS-CoV-2

One day before infection, 140 000 Calu-3 cells were seeded in respective growth medium in a 24-well plate. The next day, the medium was refreshed and cells were treated with AT, activated AT,

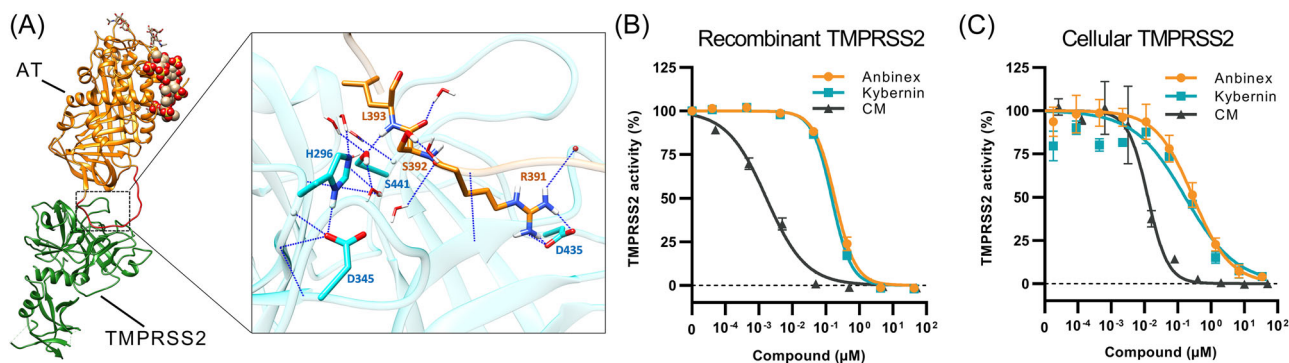


**FIGURE 1** Antithrombin inhibits TMPRSS2 protease activity. (A) Docking analysis of AT (orange, from PDB 3KCG) and TMPRSS2 (homology model, UniProtKB O15393, green). The heparin pentasaccharide is shown as spheres and glycoside residues as sticks. The inset shows the AT-TMPRSS2 catalytic complex after structural refinement. The AT RCL is depicted in orange, TMPRSS2 residues in cyan; water molecules (sticks) within a radius of 5 Å and hydrogen bonds (blue lines) are shown. (B) Recombinant TMPRSS2 (residues 106–492) was incubated with two commercially available formulations of AT (Anbinex, Kybernin) or the small molecule TMPRSS2 inhibitor CM, 1h before the addition of fluorogenic TMPRSS2 substrate BOC-QAR-AMC. Data are shown as means  $\pm$  SD derived from  $n = 2$  experiments performed in triplicates. (C) HEK293T cells expressing TMPRSS2 were incubated with AT or CM 1h before the addition of fluorogenic TMPRSS2 substrate BOC-QAR-AMC. Results were corrected for the signal of nontransfected HEK293T cells. Data are shown as means  $\pm$  SEM derived from  $n = 3$  experiments performed in duplicates. AT, antithrombin; CM, camostat mesylate; RCL, reactive center loop; SD, standard deviation; SEM, standard error of the mean.

or CM for 1 h followed by infection with SARS-CoV-2 WT (D614G) at an MOI of 0.001 for 3 h. At 3 hpi, cells were washed three times with PBS, and a growth medium supplemented with compounds was added. For treatment of cells postinfection, cells were infected for 3 h as described, washed, and treated with AT, activated AT, or CM. Supernatants were sampled after the washing step (Day 0) and at 1, 2, 3 dpi for further analysis. At each sampling time point, media were removed completely and fresh media supplemented with compounds were added.

### 2.17 | Reverse transcription-quantitative polymerase chain reaction (RT-qPCR)

To analyze SARS-CoV-2 replication by quantification of viral genome copies, viral RNA was isolated from supernatants of infected cells using the QIAamp Viral RNA Mini Kit (Qiagen) according to the manufacturer's instructions. A reaction mix consisting of 1 $\times$  Fast Virus 1-Step Mastermix (Thermo Fisher Scientific; #4444436), 0.5  $\mu$ M of each Taqman primer targeting SARS-CoV-2-ORF1b-nsp14 (fwd. primer: 5'-TGGGGYTTTACRGGTAACCT-3', rev. primer: 5'-AACRCGCTTAACAAAGCACTC-3'), 0.25  $\mu$ M probe (5'-FAM-GCAAATTGTGCAATTTG-CGG-TAMRA-3') and 5  $\mu$ l of isolated viral RNA were prepared and applied to the following cycling conditions: 1 cycle of reverse transcription (50°C, 300 s) and RT-inactivation (95°C, 20 s); 40 cycles of denaturation (95°C, 5 s) and extension (60°C, 30 s) in a Step One Plus qPCR cycler (Applied Biosystems) with Step One Software 2.3. An in-house RNA standard based on a synthetic SARS-CoV-2 RNA standard (Twist Bioscience; #102024) was used to determine genome copies from  $C_t$  values.

### 2.18 | TCID<sub>50</sub> analysis

Quantification of infectious SARS-CoV-2 titer from supernatants of infected cells was performed by TCID<sub>50</sub> analysis. To this end, 20,000 VeroE6 cells were seeded in 100  $\mu$ l respective growth medium in 96-well flat-bottom plates. The next day, 62  $\mu$ l of fresh medium were added and cells were infected in triplicates with 18  $\mu$ l of 10-fold serial dilutions of virus-containing supernatants. Upon the presence of CPE observed by light microscopy at 5–7 dpi, TCID<sub>50</sub>/ml was calculated according to the Reed–Muench formula.<sup>32</sup>

### 2.19 | Nonlinear regression and statistics

Data analysis and statistics were performed using GraphPad Prism version 9.0.2. Calculation of IC<sub>50</sub> values via nonlinear regression was performed using (normalized) response-variable slope equation. Statistical tests and  $p$  values are indicated in the respective figure legends.

## 3 | RESULTS

Proper interaction between the serpin and the protease, as well as the presence of a compatible scissile bond in the serpins RCL are prerequisites for serpin-induced protease inhibition.<sup>33</sup> To gain insight into the putative interactions of AT with TMPRSS2, we performed a computational docking analysis using a hepsin-based TMPRSS2 homology model and the crystal structure of AT (Figure 1A). Subsequent structural refinement (Supporting Information:

Figure S1a–e) revealed the formation of a hydrogen bond between the catalytic S441 of TMPRSS2 and the L393 residue of the AT RCL. This suggests that, in the AT-TMPRSS2 complex, the scissile bond in the RCL is located between residues S392 and L393, and implies an AT-mediated inhibition of TMPRSS2 (Figure 1A, inset).

To corroborate this finding, we used commercially available AT formulations, Anbinex and Kybernin, which are derived from human serum and are in clinical use for treatment of AT deficiency.<sup>34,35</sup> Both AT formulations inhibited recombinant TMPRSS2 activity in a dose-dependent manner, with IC<sub>50</sub> values of 0.18 μM for Anbinex, and 0.15 μM for Kybernin, while camostat mesylate (CM) was active in the nanomolar range (Figure 1B). The cathepsin inhibitor E64-d had no effect on TMPRSS2 activity (Supporting Information: Figure 2). Anbinex, Kybernin, and CM also inhibited the protease activity of TMPRSS2 expressed on HEK293T cells, with IC<sub>50</sub> values of 0.29, 0.17, and 0.01 μM, respectively (Figure 1C). As previously described,<sup>20</sup> AT reduced the enzymatic activity of recombinant cathepsin L, a protease involved in the endosomal activation of the SARS-CoV-2 S protein. On the other hand, AT displayed only slight activity against cathepsin B mediated cleavage (Figure 2), and did not inhibit furin, a proprotein convertase responsible for the proteolytic cleavage of the S protein at the S1/S2 and the S2' site<sup>4,5</sup> (Supporting Information: Figure 3).

We next analyzed whether AT may suppress SARS-CoV-2 Spike-driven pseudovirus entry. For this, Caco2 cells were exposed to serial dilutions of Anbinex, Kybernin, and CM, and subsequently inoculated with luciferase encoding rhabdoviral particles carrying the Wuhan/Hu-1 SARS-CoV-2 Spike. Both AT formulations suppressed Spike-driven entry with IC<sub>50</sub> values of 0.42 μM (Anbinex) and 0.43 μM (Kybernin), while CM displayed an IC<sub>50</sub> of 0.05 μM (Figure 3A).

None of the inhibitors was cytotoxic at concentrations of up to 30 μM (Supporting Information: Figure 4). AT (Anbinex) also inhibited transduction by pseudoparticles carrying Spike proteins of SARS-CoV-2 variants of concern (VoC), that is, Alpha, Beta, Gamma,

and Delta (IC<sub>50</sub> values between 0.36 and 0.83 μM) (Figure 3B). Importantly, AT also inhibited the transduction of pseudoparticles carrying the Spike of the Omicron BA.1 variant, a VoC capable of significant immune escape.<sup>36,37</sup> Inhibitory effects on Spike-driven entry were also observed for the serpin α<sub>1</sub>AT, CM, and the pan-coronavirus fusion inhibitor EK1<sup>38</sup> (Supporting Information: Figure 5A–C). Moreover, AT and CM also suppressed entry of pseudoviruses carrying Spikes of SARS-CoV, MERS- (middle east respiratory syndrome) CoV, and common cold CoV 229E, while no inhibitory effect was observed for the G protein of the vesicular stomatitis virus (VSV), a virus that does not require proteolytic activation for entry<sup>39</sup> (Figure 3C, Supporting Information: Figure 5D).

Time of addition experiments further demonstrated that AT (Anbinex) inhibited Spike-mediated entry when added before or simultaneously with the viral inoculum, but not after infection (Supporting Information: Figure 6). To exclude that components other than AT may account for the antiviral effect of Anbinex and Kybernin, both AT concentrates were subjected to a 10 kDa cutoff filter. The retentate (supposed to contain AT) and the flowthrough (supposed to contain buffer constituents such as mannitol) were collected and subsequently analyzed for protein content (Supporting Information: Figure 7A) and antiviral activity (Supporting Information: Figures 7B,C). Only the retentate but not the filtrate contained a protein band matching the size of AT (58.2 kDa) and inhibited transduction. Thus, AT inhibits SARS-CoV-2 Spike-driven viral entry at physiologically relevant concentrations.

To verify that AT also inhibits authentic SARS-CoV-2 infection, Caco2 cells were treated with AT (Anbinex) and subsequently exposed to a SARS-CoV-2 isolate Wuhan/Hu-1 (Spike mutation D614G). Flow cytometric analysis for expression of the viral nucleocapsid (N) protein 1 day later revealed a dose-dependent antiviral effect of AT with an IC<sub>50</sub> of 10.4 μM (Figure 4, Supporting Information: Figure 8). About three-fold enhanced antiviral activity of AT was observed against SARS-CoV-2 VoC Alpha (IC<sub>50</sub> 3.1 μM),

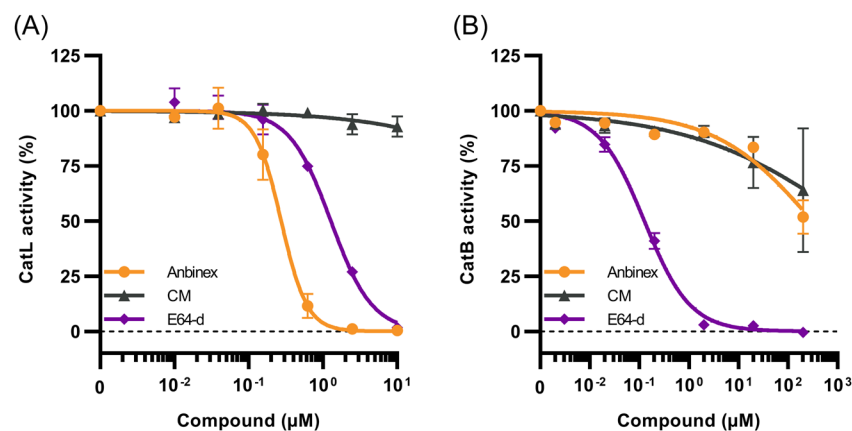


**FIGURE 2** Antithrombin inhibits activity of cathepsin L, while moderately affecting cathepsin B. Recombinant cathepsin L (A) or isolated cathepsin B (B) were incubated with AT (Anbinex), small molecule TMPRSS2 inhibitor CM or small molecule cathepsin inhibitor E64-d, 1 h before the addition of fluorogenic substrate Z-L-R-AMC (for cathepsin L) or Z-R-R-AMC (for cathepsin B). Data are shown as means ± SEM derived from  $n = 3$  experiments performed in triplicates. AT, antithrombin; CM, camostat mesylate; SEM, standard error of the mean.

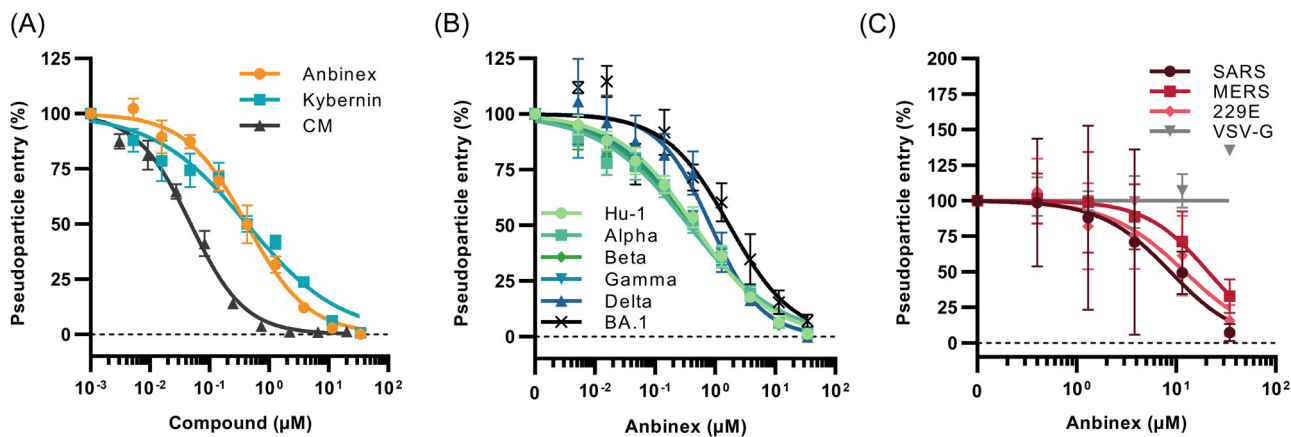


**FIGURE 3** Antithrombin inhibits coronavirus Spike-mediated entry. (A) Caco2 cells were treated with AT (Anbinex, Kybernin) or small molecule inhibitor CM for 1 h before transduction with rhabdoviral pseudoparticles carrying SARS-CoV-2 Wuhan/Hu-1 Spike. Data are shown as means  $\pm$  SEM derived from  $n = 3$  independent experiments performed in triplicates. (B) Caco2 cells were treated with AT for 1 h before transduction with lentiviral pseudoparticles carrying Spike proteins of SARS-CoV-2 VoC. Data are shown as means  $\pm$  SEM derived from  $n = 3$  independent experiments performed in triplicates. (C) Caco2 cells were treated with AT for 1 h before transduction with rhabdoviral pseudoparticles carrying the indicated glycoproteins. Data are shown as means  $\pm$  SD derived from  $n = 2$  experiments performed in quadruplicates. Pseudoparticle entry rates were assessed by measuring luciferase activity in cell lysates at 48 h (lentiviral pseudoparticles) or at 16 h (rhabdoviral pseudoparticles) post transduction. AT, antithrombin; CM, camostat mesylate; SD, standard deviation; SEM, standard error of mean; VoC, variants of concern.

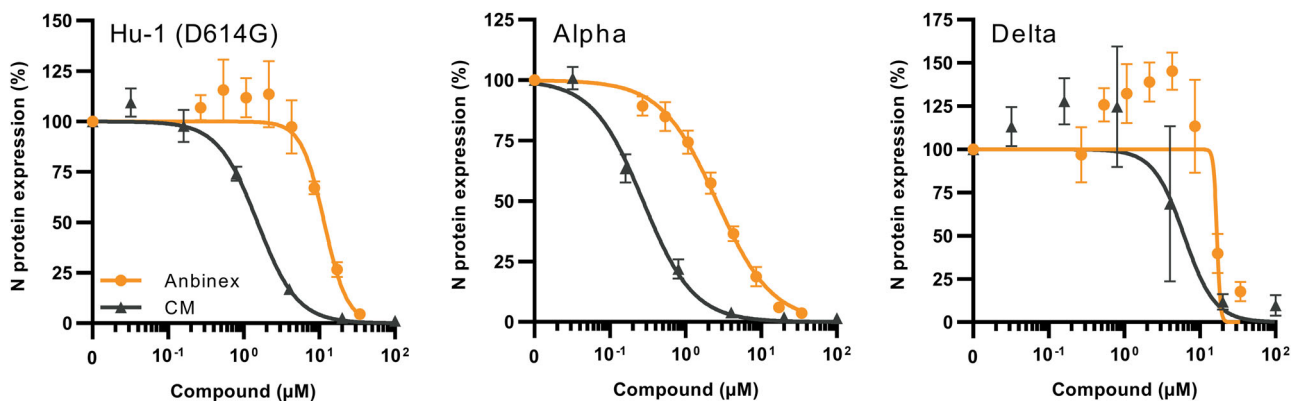


**FIGURE 4** Antithrombin reduces SARS-CoV-2 infection. Caco2 cells were treated with AT (Anbinex) or small molecule inhibitor CM for 1 h before infection with SARS-CoV-2 isolates Wuhan/Hu-1 (Spike mutation D614G) or VoC Alpha and Delta at an MOI of 0.005. Infection rates were assessed by flow cytometric analysis of SARS-CoV-2 nucleocapsid (N) protein expression at 1 dpi. Signal from PBS-treated, infected cells served as control and was used for normalization. Data are shown as means  $\pm$  SEM derived from  $n = 3$  independent experiments. AT, antithrombin; CM, camostat mesylate; MOI, multiplicity of infection; PBS, phosphate-buffered saline; SEM, standard error of the mean; VoC, variants of concern.

while VoC Delta was inhibited with an  $IC_{50}$  of 13.9  $\mu$ M. About 10-fold higher antiviral activities were observed for CM ( $IC_{50}$  values of 1.5, 0.2, and 6.2  $\mu$ M, respectively). Whether the differences in the  $IC_{50}$ s of CM and AT against the different SARS-CoV-2 strains are due to different TMPRSS2 dependency or other factors remains to be determined. Taken together, AT inhibits the activity of TMPRSS2 and prevents authentic SARS-CoV-2 infection.

AT-mediated inhibition of target proteases (mainly factor Xa) is potentiated by heparin or heparin-derived agents such as the pentasaccharide Fondaparinux (FPX).<sup>40,41</sup> Heparin and FPX are in routine clinical use as anticoagulant medication. Both molecules bind

to an allosteric site of AT and induce a more pronounced exposition and flexibility of the AT RCL, leading to an increased antiprotease activity.<sup>42</sup> Indeed, incubation of AT with heparin or FPX enhanced inhibition of recombinant TMPRSS2 enzyme activity (Figure 5A). Interestingly, only FPX significantly increased inhibition of cell-associated TMPRSS2 activity by AT (Figure 5B). In contrast to previously published data, activated AT had no effect on furin activity<sup>43</sup> (Supporting Information: Figure 9). Of note, heparin or FPX alone neither affected cell-free (Supporting Information: Figure 10A) nor cell-associated (Supporting Information: Figure 10B) TMPRSS2 activity.

We then studied whether heparin and FPX may confer antiviral activity to an Anbinex concentration otherwise insufficient to reduce authentic SARS-CoV-2 infection (Figure 5). Flow cytometric quantification of N-positive cells revealed ~45% reduced infection rates for the maximum heparin concentration applied (22.2  $\mu$ M). In comparison, activation with  $\geq 9.3$   $\mu$ M of FPX inhibited genuine SARS-CoV-2 infection almost entirely (Figure 5C). Heparin or FPX alone did not reduce SARS-CoV-2 infection (Supporting Information: Figure 10C). Similarly, activation of a non-antiviral Kyberlin concentration by FPX but not heparin resulted in almost complete inhibition of SARS-CoV-2 infection (Supporting Information: Figure 11). As shown in Figure 5D, FPX also increased the antiviral activity of AT against SARS-CoV-2 VOCs Alpha and Delta. These data show that activated AT is a highly potent inhibitor of SARS-CoV-2 infection. Thus, FPX-mediated activation of AT boosts the inhibitory effect on SARS-CoV-2 infection.

To determine whether AT also inhibits SARS-CoV-2 replication (i.e., multiple rounds of infection) in human lung cells, Calu-3 cells were treated with AT (13.8  $\mu$ M), FPX-activated AT (13.8  $\mu$ M), FPX alone, or CM (100  $\mu$ M) and then infected with a low MOI of SARS-CoV-2 (day 0, inoculum). The entire supernatants were collected on Days 1, 2, and 3 and replaced by fresh medium containing the respective compounds. Viral RNA copies were determined by qPCR and revealed an exponential growth in the mock control from  $10^5$  RNA copies (inoculum) to more than  $10^9$  RNA copies on Day 3 post-infection (Figure 6A). AT (Anbinex) and CM markedly reduced SARS-CoV-2 replication (Figure 6A). Notably, FPX-activated AT prevented viral replication almost entirely, while FPX alone displayed no antiviral activity (Figure 6A). Analysis of cumulative viral RNA copy production revealed a more than 340- (>99.7%) and 2400-fold (>99.99%) reduction by AT or activated AT, respectively. In

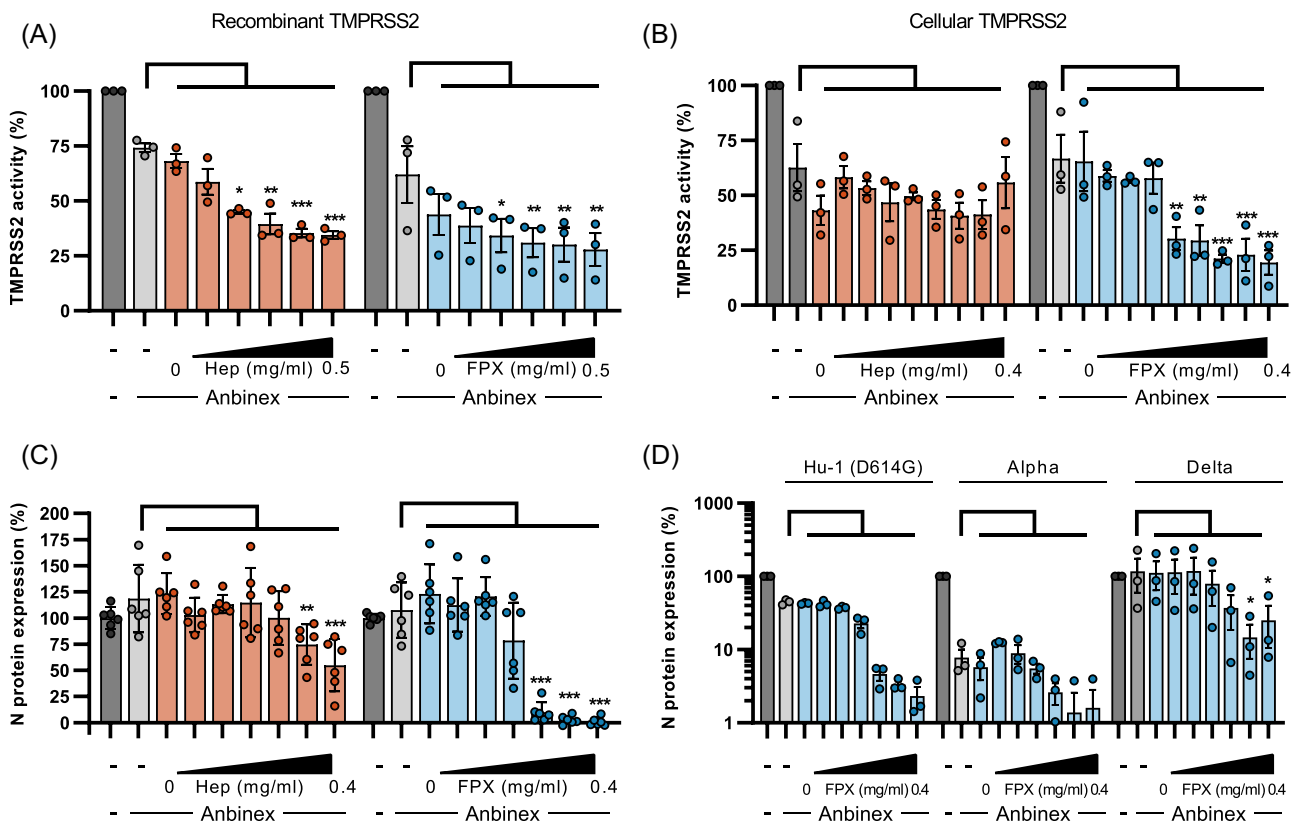


**FIGURE 5** Activation of antithrombin increases anti-TMPRSS2 and anti-SARS-CoV-2 activity. (A) Heparin (Hep)- and Fondaparinux (FPX)-activated antithrombin (Anbinex, 0.0137  $\mu$ M) was incubated with recombinant TMPRSS2 enzyme before the addition of fluorogenic TMPRSS2 substrate BOC-QAR-AMC. Data are shown as means  $\pm$  SEM derived from  $n = 3$  experiments performed in triplicates. (B) HEK293T cells expressing TMPRSS2 were incubated with Hep- or FPX-activated Anbinex (0.17  $\mu$ M) before the addition of fluorogenic TMPRSS2 substrate BOC-QAR-AMC. Results were corrected for the signal of nontransfected HEK293T cells. Data are shown as means  $\pm$  SEM derived from  $n = 3$  experiments performed in duplicates. (C) Caco2 cells were treated with Hep- or FPX-activated Anbinex (13.75  $\mu$ M) for 1 h before infection of cells with SARS-CoV-2 isolate Wuhan/Hu-1 (Spike mutation D614G) at an MOI of 0.0002. Data are shown as means  $\pm$  SD derived from  $n = 2$  experiments performed in triplicates. (D) Caco2 cells were treated with FPX-activated Anbinex (13.75  $\mu$ M) for 1 h before infection of cells with the indicated SARS-CoV-2 isolates at an MOI of 0.005. Data are shown as means  $\pm$  SEM derived from  $n = 3$  experiments. Infection rates of (C) and (D) were assessed by flow cytometric analysis of SARS-CoV-2 nucleocapsid (N) protein expression in single cells at 2 dpi (C) or 1 dpi (D). Maximum final concentrations of Hep and FPX on cells were 0.4 mg/ml, corresponding to 22.2 or 232  $\mu$ M, respectively. \* $p \leq 0.05$ , \*\* $p \leq 0.01$ , \*\*\* $p \leq 0.001$ , assessed by two-way analysis of variance with Dunnett's multiple comparisons test. MOI, multiplicity of infection; SD, standard deviation; SEM, standard error of the mean.



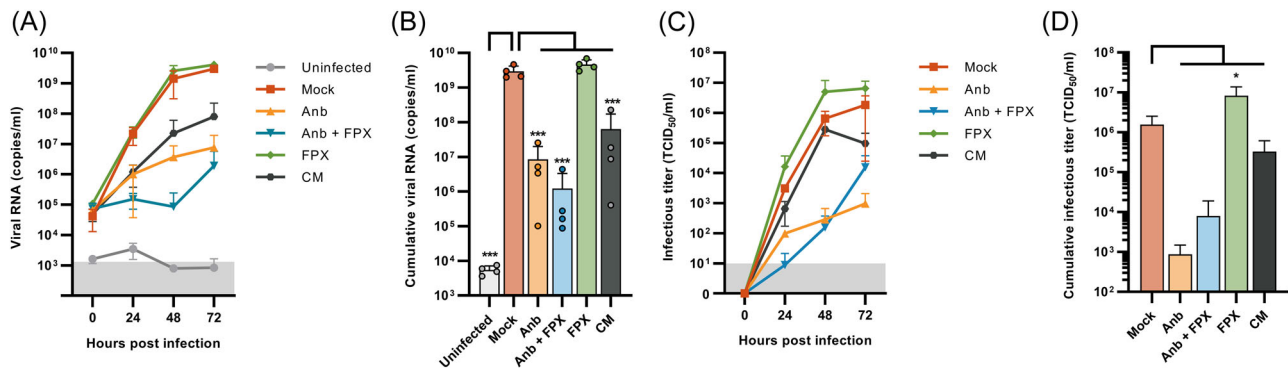


**FIGURE 6** Activated antithrombin reduces SARS-CoV-2 replication in human lung cells. Calu-3 cells were treated with AT (Anb, Anbinex, 13.75  $\mu$ M), FPX activated AT, FPX or small molecule inhibitor CM (100  $\mu$ M) for 1h before infection with SARS-CoV-2 isolate Wuhan/Hu-1 (Spike mutation D614G) at an MOI of 0.001. 3 h later, the inoculum was removed, cells were washed and fresh medium supplemented with respective compounds was added. Complete supernatants were sampled at 0, 24, 48, and 72 h postinfection (hpi) and fresh medium with compound added after sampling. (A) RT-qPCR targeting SARS-CoV-2 ORF1b nsp14 of harvested supernatants. (B) Cumulative SARS-CoV-2 RNA copies until 3 dpi assessed by area under the curve analysis of harvested supernatants. (C) TCID<sub>50</sub> analysis of harvested supernatants. (D) Cumulative infectious virus yield assessed by area under the curve analysis of timepoints until 3 dpi from (C). Gray areas indicate the limit of quantification. Data are shown as mean  $\pm$  SD from  $n = 2$  experiments performed in duplicates. \* $p \leq 0.05$ , \*\* $p \leq 0.01$ , \*\*\* $p \leq 0.001$ , assessed by ordinary one-way analysis of variance with Dunnett's multiple comparisons test. AT, antithrombin; CM, camostat mesylate; FPX, fondaparinux; MOI, multiplicity of infection, RT-qPCR, reverse transcription-quantitative polymerase chain reaction; SARS-CoV-2, severe acute respiratory syndrome coronavirus 2; SD, standard deviation.

comparison, CM reduced viral RNA by  $\sim$ 45-fold (97.8%) (Figure 6B). Accordingly, the infectious titers in the supernatants of mock- or FPX-treated cells peaked at 3 dpi and were reduced by AT and FPX-activated AT and—to a lesser extent—by CM (Figure 6C). Overall, the infectious titer was reduced by 5-fold (79.1%) by CM, 1800-fold (99.94%) by AT alone, and 200-fold (99.5%) through FPX-activated AT (Figure 6D). Similar results were obtained in a more therapeutic setting when Calu-3 cells were treated with the respective compounds after infection with SARS-CoV-2 (Supporting Information: Figure 12). Thus, AT inhibits SARS-CoV-2 infection and replication in lung epithelial cells.

## 4 | DISCUSSION

TMPRSS2 has been established as a critical determinant of SARS-CoV-2 tropism and pathogenesis.<sup>44</sup> The physiological concentration of AT in plasma is  $\sim$ 2.6  $\mu$ M.<sup>16</sup> This concentration is well sufficient to block Spike-driven entry of pseudoparticles (IC<sub>50</sub> of  $\sim$ 0.4  $\mu$ M). AT concentrations required to prevent authentic SARS-CoV-2 infection and replication were higher, with IC<sub>50</sub> values around 3  $\mu$ M. In most infected individuals, SARS-CoV-2 mainly replicates in the upper and lower respiratory tract.<sup>45</sup> Since AT is largely absent from the airways, it does most likely not protect against the acquisition of SARS-CoV-2. However, systemic concentrations of AT may limit the extrapulmonary spread of SARS-CoV-2 to distinct organs and hence prevent severe COVID-19. It would thus be intriguing to investigate whether serum AT levels and viral loads are inversely correlated to reveal a potential role of AT in the extrapulmonary spread of SARS-CoV-2. Moreover, AT binds to heparin or heparan sulfate-containing

glycosaminoglycans (GAGs), which are present on the surface of most cells. AT-GAG interaction results in increased anti-proteolytic activity of AT<sup>46–50</sup> which may also result in an increased anti-TMPRSS2 and consequently anti-SARS-CoV-2 activity. Our finding that AT is a potent inhibitor of TMPRSS2 activity and SARS-CoV-2 entry is in accordance with recently published data showing activity of SerpinA1, SerpinC1 (AT), and SerpinE1 on SARS-CoV-2 Spike cleavage and entry<sup>51</sup> and suggests that this endogenous serpin may play a role in SARS-CoV-2 systemic spread and disease progression *in vivo*.

Molecular modeling and biochemical experiments with recombinant and cell-associated TMPRSS2 demonstrated that AT is an inhibitor of TMPRSS2, a serine protease that is involved in the regulation of several signaling molecules and receptors but of unknown physiological function.<sup>52–55</sup> Many viral pathogens utilize TMPRSS2 as an entry cofactor and exploit its proteolytic activity to prime their glycoproteins for subsequent fusion. Consequently, inhibition of TMPRSS2 enzyme activity by, for example, CM or  $\alpha_1$ AT prevents processing of viral glycoprotein and subsequent infection.<sup>12,56–58</sup> Likewise, AT suppressed SARS-CoV-2, SARS-CoV, MERS-CoV, and common cold CoV-229E Spike-driven entry, as shown herein. TMPRSS2 is also utilized by other coronaviruses, but also certain influenza A virus strains, as well as parainfluenza-, metapneumo- and sendaiviruses.<sup>59–68</sup> Intriguingly, AT also inhibits cathepsin L, a lysosomal and cell-free cysteine protease shown to prime SARS-CoV-2 Spike and promote cell-cell fusion.<sup>69</sup> Thus, it is plausible to speculate that AT may act as a broad-spectrum inhibitor against different viral pathogens by blocking essential host cell proteases. Testing the antiviral efficacy of native or activated AT against respiratory viruses *in vitro* and *in vivo* is highly warranted.

AT is a clinically approved anticoagulant in patients with hereditary and acquired antithrombin deficiency<sup>70</sup> suggesting that repurposing AT for therapy of SARS-CoV-2/COVID-19 should be considered. AT as a drug is available as purified protein from human plasma (e.g., Anbixin or Kybernin used herein),<sup>71</sup> and is administered intravenously. COVID-19 is associated with coagulation abnormalities and often results in coagulopathy associated with severe disease.<sup>72-76</sup> Of note, previous studies reported that severe or fatal COVID-19 is linked with decreased AT levels.<sup>77-84</sup> The interrelation of AT levels, coagulation parameters, and COVID-19 severity is the subject of a recently initiated, retrospective clinical trial comparing COVID-19 patients who received AT supplementation to those that did not (NCT04651400). AT augmentation therapy of COVID-19 patients may on the one hand directly interfere with SARS-CoV-2 replication due to its antiviral activity and on the other hand, reduce coagulopathy. Currently, a clinical trial (NCT04745442) is investigating whether intravenous AT supplementation attenuates or even curbs COVID-19-related inflammation and coagulopathy. Our results strongly suggest that increased AT levels will also exert beneficial effects by direct inhibition of SARS-CoV-2 replication.

Our data further suggest that activation of AT with the synthetic pentasaccharide FPX and—to a lesser extent—heparin increases its anti-TMPRSS2 and antiviral activity. Mechanistically, this infers that the expulsion of the AT RCL, rather than the formation of the ternary complex between protease, antiprotease, and its activator, is responsible for this effect. A recent study described a reduction of electrostatic repulsions between the serpin  $\alpha_1$ AT and the low molecular weight heparin (LMWH) enoxaparin,<sup>85</sup> which might also contribute to the activation of AT. Heparin or LMWH are administered as the standard of care in the majority of COVID-19 patients at daily intravenous doses of several thousand international units (IU), while FPX is administered at 2.5 mg, respectively.<sup>74,80,86</sup> Although previous reports on the use of AT in patients unresponsive to escalated doses of heparin showed favorable outcomes,<sup>87-94</sup> it remains to be clarified how the presence of anticoagulants affects the activity of supplemented AT with respect to a potential treatment of COVID-19. Inhalative administration of native or activated AT early during infection might be superior to systemic application for treatment of COVID-19 since it directly targets the main replication site of the virus and circumvents a potential risk of systemic bleeding. Application of nebulized AT alone or in combination with heparin has been described in a rat model of acute lung injury and was found to reduce lung permeability, inflammation and attenuate pulmonary coagulopathy.<sup>95,96</sup> In conclusion, the antiviral effect of AT described herein, together with the well-described anticoagulant and anti-inflammatory properties, strengthens the call for clinical studies on therapeutic AT for treatment of COVID-19<sup>97</sup> and other respiratory pathogens.

#### AUTHOR CONTRIBUTIONS

Lukas Wettstein and Patrick Immenschuh designed most experiments and performed SARS-CoV-2 pseudoparticle experiments, toxicity

studies, cell-associated, and recombinant TMPRSS2 activity studies; Tatjana Weil and Carina Conzelmann performed authentic SARS-CoV-2 studies; Steffen Stenger supervised work in the BSL3; Yasser Almeida-Hernández and Elsa Sanchez-Garcia performed the computational studies and analyzed the results; Markus Hoffmann, Amy Kempf, Inga Nehlmeier, and Stefan Pöhlmann performed and evaluated SARS-CoV, MERS-CoV, and 229E Spike experiments and recombinant TMPRSS2 assay. Rishikesh Lotke, Moritz Petersen, and Daniel Sauter performed the furin reporter assay and provided reagents for it, respectively. Lukas Wettstein, Elsa Sanchez-Garcia, and Jan Münch wrote the paper.

#### ACKNOWLEDGMENTS

L. W., C. C., and T. W. are part of the International Graduate School in Molecular Medicine Ulm. We thank Daniela Krnavek, Isabell Haußmann and Nicola Schrott for expert technical assistance. J. M. acknowledges funding by the German Research Foundation (DFG) through “Fokus-Förderung COVID-19” (FR 2974/3-1, KL 2544/8-1), the EU’s Horizon 2020 research and innovation programme (Fight-nCoV, 101003555 to J. M.) and the Sonderfördermassnahme COVID-19 of the MWK Baden-Württemberg, Germany. J. M and E. S.-G. are funded by the DFG within the CRC 1279 “Exploiting the Human Peptidome for Novel Antimicrobial and Anticancer Agents.” E. S.-G. further acknowledges the DFG under Germany’s Federal and State Excellence Strategy EXC- 2033 Projektnummer 390677874 and the major instrumentation granted under the DFG—Projektnummer: 436586093. S. P. was supported by BMBF (RAPID Consortium, 01KI1723D, and 01KI2006D; RENACO, 01KI20328A, 01KI20396). D. S. is supported by the BMBF (01KI20135) and the Heisenberg Programme of the DFG. M. P. receives funding from the DZIF and would like to thank the Interdisciplinary Doctoral Programme in Medicine of the Medical Faculty of Tübingen University for support. Open Access funding enabled and organized by Projekt DEAL.

#### CONFLICT OF INTEREST

The authors declare no conflict of interest.

#### DATA AVAILABILITY STATEMENT

The data that support the findings of this study are available from the corresponding author upon reasonable request. The initial coordinates were obtained from the SWISS-MODEL repository (<https://swissmodel.expasy.org/repository/uniprot/O15393>) and the Protein Data Bank accession code PDB ID: 3KCG. Source data are provided with this paper.


#### ORCID

Lukas Wettstein  <https://orcid.org/0000-0002-8182-9309>

Patrick Immenschuh  <https://orcid.org/0000-0001-6894-1198>

Tatjana Weil  <https://orcid.org/0000-0003-0925-2426>

Carina Conzelmann  <https://orcid.org/0000-0002-0752-3678>

Yasser Almeida-Hernández  <https://orcid.org/0000-0001-9832-3534>

## REFERENCES

- Batista C, Shoham S, Ergonul O, et al. Urgent needs to accelerate the race for COVID-19 therapeutics. *EClinicalMedicine*. 2021;36:100911.
- Shang J, Wan Y, Luo C, et al. Cell entry mechanisms of SARS-CoV-2. *Proc Natl Acad Sci USA*. 2020;117:11727-11734.
- V'kovski P, Kratzel A, Steiner S, Stalder H, Thiel V. Coronavirus biology and replication: implications for SARS-CoV-2. *Nat Rev Microbiol*. 2020;19:155-170. doi:10.1038/s41579-020-00468-6
- Essalmani R, Jain J, Susan-Resiga D, et al. Distinctive roles of Furin and TMPRSS2 in SARS-CoV-2 infectivity. *J Virol*. 2022;96:e0012822.
- Hoffmann M, Kleine-Weber H, Schroeder S, et al. SARS-CoV-2 cell entry depends on ACE2 and TMPRSS2 and is blocked by a clinically proven protease inhibitor. *Cell*. 2020;181:271-280.e8.
- Millet JK, Whittaker GR. Physiological and molecular triggers for SARS-CoV membrane fusion and entry into host cells. *Virology*. 2018;517:3-8.
- Hoffmann M, Hofmann-Winkler H, Smith JC, et al. Camostat mesylate inhibits SARS-CoV-2 activation by TMPRSS2-related proteases and its metabolite GBPA exerts antiviral activity. *EBioMedicine*. 2021;65, 103255.
- Li K, Meyerholz DK, Bartlett JA, McCray PB. The Tmprss2 inhibitor nafamostat reduces SARS-CoV-2 pulmonary infection in mouse models of COVID-19. *mBio*. 2021;12:e0097021.
- Hoffmann M, Schroeder S, Kleine-Weber H, Müller MA, Drosten C, Pöhlmann S. Nafamostat mesylate blocks activation of SARS-CoV-2: new treatment option for COVID-19. *Antimicrob Agents Chemother*. 2020;64:19-21.
- Hoffmann M, Arora P, Groß R, et al. SARS-CoV-2 variants B.1.351 and P.1 escape from neutralizing antibodies. *Cell*. 2021;184:2384-2393.e12.
- Yamamoto M, Kiso M, Sakai-Tagawa Y, et al. The anticoagulant nafamostat potently inhibits SARS-CoV-2 S protein-mediated fusion in a cell fusion assay system and viral infection in vitro in a cell-type-dependent manner. *Viruses*. 2020;12, 629.
- Wettstein L, Weil T, Conzelmann C, et al. Alpha-1 antitrypsin inhibits TMPRSS2 protease activity and SARS-CoV-2 infection. *Nat Commun*. 2021;12:1726.
- Azouz NP, Klingler AM, Callahan V, et al. Alpha 1 antitrypsin is an inhibitor of the SARS-CoV-2-priming protease TMPRSS2. *Pathog Immun*. 2021;6:55-74.
- Heit C, Jackson BC, McAndrews M, et al. Update of the human and mouse SERPIN gene superfamily. *Hum Genomics*. 2013;7:22.
- Mangan MSJ, Kaiserman D, Bird PI. The role of serpins in vertebrate immunity. *Tissue Antigens*. 2008;72:1-10. Preprint at doi:10.1111/j.1399-0039.2008.01059.x
- Conard J, Brosstad F, Lie Larsen M, Samama M, Abildgaard U. Molar antithrombin concentration in normal human plasma. *Haemostasis*. 1983;13:363-368.
- Björk I, Olson ST. *Chemistry and Biology of Serpins, Antithrombin—A Bloody Important Serpin*. Springer; 1997.
- Levy JH, Sniecinski RM, Welsby IJ, Levi M. Antithrombin: anti-inflammatory properties and clinical applications. *Thromb Haemost*. 2016;115:712-728.
- Danielsson Å, Björk I. Mechanism of inactivation of trypsin by antithrombin. *Biochem J*. 1982;207:21-28.
- Björk I, Nordling K, Raub-Segall E, Hellman U, Olson ST. Inactivation of papain by antithrombin due to autolytic digestion: a model of serpin inactivation of cysteine proteinases. *Biochem J*. 1998;335:701-709.
- Khan MS, Singh P, Azhar A, et al. Serpin inhibition mechanism: a delicate balance between native metastable state and polymerization. *J Amino Acids*. 2011;2011:1-10.
- Huntington JA. Serpin structure, function and dysfunction. *J Thromb Haemostasis*. 2011;9:26-34.
- Waterhouse A, Bertoni M, Bienert S, et al. SWISS-MODEL: homology modelling of protein structures and complexes. *Nucleic Acids Res*. 2018;46:W296-W303.
- Johnson DJD, Langdown J, Huntington JA. Molecular basis of factor IXa recognition by heparin-activated antithrombin revealed by a 1.7-Å structure of the ternary complex. *Proc Natl Acad Sci USA*. 2010;107:645-650.
- Van Zundert GCP, Rodrigues J, Trellet M, et al. The HADDOCK2.2 web server: user-friendly integrative modeling of biomolecular complexes. *J Mol Biol*. 2016;428:720-725.
- Heo L, Park H, Seok C. GalaxyRefine: protein structure refinement driven by side-chain repacking. *Nucleic Acids Res*. 2013;41:384-388.
- Heo L, Lee H, Seok C. GalaxyRefineComplex: refinement of protein-protein complex model structures driven by interface repacking. *Sci Rep*. 2016;6:1-10.
- Chaudhury S, Berrondo M, Weitzner BD, Muthu P, Bergman H, Gray JJ. Benchmarking and analysis of protein docking performance in Rosetta v3.2. *PLoS One*. 2011;6, 22477.
- Best RB, Zhu X, Shim J, et al. Optimization of the additive CHARMM all-atom protein force field targeting improved sampling of the backbone  $\phi$ ,  $\psi$  and side-chain  $\chi_1$  and  $\chi_2$  Dihedral Angles. *J Chem Theory Comput*. 2012;8:3257-3273.
- Abraham MJ, Murtola T, Schulz R, et al. Gromacs: high performance molecular simulations through multi-level parallelism from laptops to supercomputers. *SoftwareX*. 2015;1-2:19-25.
- Rentsch MB, Zimmer G. A vesicular stomatitis virus replicon-based bioassay for the rapid and sensitive determination of multi-species type I interferon. *PLoS One*. 2011;6:e25858.
- Reed LJ, Muench H. A simple method of estimating fifty per cent endpoints. *Am J Epidemiol*. 1938;27:493-497.
- Gettins PGW. Serpin structure, mechanism, and function. *Chem Rev*. 2002;102:4751-4804. doi:10.1021/cr010170
- Grifols SA Anbinex [package insert]. (Preprint at 2017).
- Behring CSL. Kybernin [package insert]. (Preprint at 2018).
- Hoffmann M, Krüger N, Schulz S, Cossmann A. The Omicron variant is highly resistant against antibody-mediated neutralization—implications for control of the COVID-19 pandemic. *Cell*. 2021;185:447-456.
- Karim SSA, Karim QA. Omicron SARS-CoV-2 variant: a new chapter in the COVID-19 pandemic. *Lancet*. 2021;398:2126-2128.
- Xia S, Yan L, Xu W, et al. A pan-coronavirus fusion inhibitor targeting the HR1 domain of human coronavirus spike. *Sci Adv*. 2019;5:eav4580.
- Sun X, Roth SL, Bialecki MA, Whittaker GR. Internalization and fusion mechanism of vesicular stomatitis virus and related rhabdoviruses. *Future Virol*. 2010;5:85-96.
- Bauer KA, Hawkins DW, Peters PC, et al. Fondaparinux, a synthetic pentasaccharide: the first in a new class of antithrombotic agents—the selective factor Xa inhibitors. *Cardiovasc Drug Rev*. 2002;20:37-52.
- Turpie AGG, Lassen MR, Eriksson BI, Bauer KA. Factor Xa inhibitors in the prevention and treatment of venous thromboembolism—the role of fondaparinux, first of a new class of antithrombotic agents. *Today Ther Trends*. 2002;20:253-267.
- Walenga JM, Jeske WP, Samama MM, Frapaise FX, Bick RL, Fareed J. Fondaparinux: a synthetic heparin pentasaccharide as a new antithrombotic agent. *Expert Opin Invest Drugs*. 2002;11:397-407.
- Brennan SO, Nakayama K. Furin has the proalbumin substrate specificity and serpin inhibitory properties of an in situ hepatic convertase. *FEBS Lett*. 1994;338:147-151.
- Millet JK, Whittaker GR. Host cell proteases: critical determinants of coronavirus tropism and pathogenesis. *Virus Res*. 2015;202:120-134.
- Hou YJ, Okuda K, Edwards CE, et al. SARS-CoV-2 reverse genetics reveals a variable infection gradient in the respiratory tract. *Cell*. 2020;182:429-446.e14.

46. Weitz JI. Low-molecular-weight heparins. *N Engl J Med.* 1997;337:688-698.
47. Rosenberg RD. The heparin-antithrombin system: a natural anticoagulant mechanism. *J Clin Invest.* 1994;74:1-6.
48. Quinsey NS, Greedy AL, Bottomley SP, Whisstock JC, Pike RN. Antithrombin: in control of coagulation. *Int J Biochem Cell Biol.* 2004;36:386-389.
49. Olson ST, Swanson R, Raub-Segall E, et al. Accelerating ability of synthetic oligosaccharides on antithrombin inhibition of proteinases of the clotting and fibrinolytic systems. Comparison with heparin and low-molecular-weight heparin. *Thromb Haemost.* 2004;92:929-939.
50. Jin L, Abrahams JP, Skinner R, Petitou M, Pike RN, Carrell RW. The anticoagulant activation of antithrombin by heparin. *Proc Natl Acad Sci USA.* 1997;94:14683-14688.
51. Rosendal E, Mihai IS, Becker M, et al. Serine protease inhibitors restrict host susceptibility to SARS-CoV-2 infections. *mBio.* 2022, 13:e0089222. doi:10.1128/mbio.00892-22
52. Lucas JM, Heinlein C, Kim T, et al. The androgen-regulated protease TMPRSS2 activates a proteolytic cascade involving components of the tumor microenvironment and promotes prostate cancer metastasis. *Cancer Discov.* 2014;4:1310-1325.
53. Donaldson SH, Hirsh A, Li DC, et al. Regulation of the epithelial sodium channel by serine proteases in human airways. *J Biol Chem.* 2002;277:8338-8345.
54. Wilson S, Greer B, Hooper J, et al. The membrane-anchored serine protease, TMPRSS2, activates PAR-2 in prostate cancer cells. *Biochem J.* 2005;388:967-972.
55. Mackie EJ, Pagel CN, Smith R, de Niese MR, Song SJ, Pike RN. Protease-activated receptors: a means of converting extracellular proteolysis into intracellular signals. *IUBMB Life.* 2002;53:277-281.
56. Hempel T, Raich L, Olsson S, et al. Molecular mechanism of inhibiting the SARS-CoV-2 cell entry facilitator TMPRSS2 with camostat and nafamostat. *Chem Sci.* 2021;12:983-992.
57. Kleine-Weber H, Elzayat M, Hoffmann M, Pöhlmann S. Functional analysis of potential cleavage sites in the MERS-coronavirus spike protein. *Sci Rep.* 2018;8:1-11.
58. Kawase M, Shirato K, van der Hoek L, Taguchi F, Matsuyama S. Simultaneous treatment of human bronchial epithelial cells with serine and cysteine protease inhibitors prevents severe acute respiratory syndrome coronavirus entry. *J Virol.* 2012;86:6537-6545.
59. Bestle D, Limburg H, Kruhl D, et al. Hemagglutinins of Avian influenza viruses are proteolytically activated by TMPRSS2 in human and Murine airway cells. *J Virol.* 2021;95:e0090621.
60. Böttcher E, Matrosovich T, Beyerle M, Klenk HD, Garten W, Matrosovich M. Proteolytic activation of influenza viruses by serine proteases TMPRSS2 and HAT from human airway epithelium. *J Virol.* 2006;80:9896-9898.
61. Galloway SE, Reed ML, Russell CJ, Steinhauer DA. Influenza HA subtypes demonstrate divergent phenotypes for cleavage activation and pH of fusion: implications for host range and adaptation. *PLoS Pathog.* 2013;9, 1003151.
62. Hatesuer B, Bertram S, Mehnert N, et al. TMPRSS2 is essential for influenza H1N1 virus pathogenesis in mice. *PLoS Pathog.* 2013;9:e1003774.
63. Bertram S, Dijkman R, Habjan M, et al. TMPRSS2 activates the human coronavirus 229E for cathepsin-independent host cell entry and is expressed in viral target cells in the respiratory epithelium. *J Virol.* 2013;87:6150-6160.
64. Kawase M, Shirato K, Matsuyama S, Taguchi F. Protease-mediated entry via the endosome of human coronavirus 229E. *J Virol.* 2009;83:712-721.
65. Shirato K, Kanou K, Kawase M, Matsuyama S. Clinical isolates of human coronavirus 229E bypass the endosome for cell entry. *J Virol.* 2017;91:e01387-16.
66. Shirato K, Kawase M, Matsuyama S. Wild-type human coronaviruses prefer cell-surface TMPRSS2 to endosomal cathepsins for cell entry. *Virology.* 2018;517:9-15.
67. Abe M, Tahara M, Sakai K, et al. TMPRSS2 is an activating protease for respiratory parainfluenza viruses. *J Virol.* 2013;87:11930-11935.
68. Shirogane Y, Takeda M, Iwasaki M, et al. Efficient multiplication of human metapneumovirus in vero cells expressing the transmembrane serine protease TMPRSS2. *J Virol.* 2008;82:8942-8946.
69. Zhao MM, Yang WL, Yang FY, et al. Cathepsin L plays a key role in SARS-CoV-2 infection in humans and humanized mice and is a promising target for new drug development. *Signal Transduct Target Ther.* 2021;6, 134.
70. Rodgers G. Role of antithrombin concentrate in treatment of hereditary antithrombin deficiency. *Thromb Haemost.* 2009;101:806-812.
71. Wong TE, Huang YS, Weiser J, Brogan TV, Shah SS, Witmer CM. Antithrombin concentrate use in children: a multicenter cohort study. *J Pediatr.* 2013;163:1329-1334.e1.
72. Cui S, Chen S, Li X, Liu S, Wang F. Prevalence of venous thromboembolism in patients with severe novel coronavirus pneumonia. *J Thromb Haemostasis.* 2020;18:1421-1424.
73. Klok FA, Kruip M, van der Meer N, et al. Incidence of thrombotic complications in critically ill ICU patients with COVID-19. *Thromb Res.* 2020;191:145-147.
74. White D, MacDonald S, Bull T, et al. Heparin resistance in COVID-19 patients in the intensive care unit. *J Thromb Thrombolysis.* 2020;50:287-291.
75. Polimeni A, Leo I, Spaccarotella C, et al. Differences in coagulopathy indices in patients with severe versus non-severe COVID-19: a meta-analysis of 35 studies and 6427 patients. *Sci Rep.* 2021;11:1-10.
76. Helms J, Tacquard C, Severac F, et al. High risk of thrombosis in patients with severe SARS-CoV-2 infection: a multicenter prospective cohort study. *Intensive Care Med.* 2020;46:1089-1098.
77. Gazzaruso C, Paolozzi E, Valenti C, et al. Association between antithrombin and mortality in patients with COVID-19. A possible link with obesity. *Nutr Metab Cardiovasc Dis.* 2020;30:1914-1919.
78. Anakli İ, Ergin Özcan P, Polat Ö, et al. Prognostic value of antithrombin levels in COVID-19 patients and impact of fresh frozen plasma treatment: a retrospective study. *Turk J Haematol.* 2021;38:15-21.
79. Martín-Rojas RM, Pérez-Rus G, Delgado-Pinos VE, et al. COVID-19 coagulopathy: an in-depth analysis of the coagulation system. *Eur J Haematol.* 2020;105:741-750.
80. Nougier C, Benoit R, Simon M, et al. Hypofibrinolytic state and high thrombin generation may play a major role in SARS-COV2 associated thrombosis. *J Thromb Haemostasis.* 2020;18:2215-2219.
81. Zhang Q, Chen CZ, Swaroop M, et al. Heparan sulfate assists SARS-CoV-2 in cell entry and can be targeted by approved drugs in vitro. *Cell Discov.* 2020;6, 80.
82. Liao D, Zhou F, Luo L, et al. Haematological characteristics and risk factors in the classification and prognosis evaluation of COVID-19: a retrospective cohort study. *Lancet Haematol.* 2020;7:e671-e678.
83. Han H, Yang L, Liu R, et al. Prominent changes in blood coagulation of patients with SARS-CoV-2 infection. *Clin Chem Lab Med.* 2020;58:1116-1120.
84. Tritschler T, Mathieu ME, Skeith L, et al. Incidence of venous thromboembolism in hospitalized patients with COVID-19. *J Thromb Haemostasis.* 2020;18:1995-2002.
85. Bai X, Buckle AM, Vladar EK, et al. Enoxaparin augments alpha-1-antitrypsin inhibition of TMPRSS2, a promising drug combination against COVID-19. *Sci Rep.* 2022;12:5207.
86. Russo V, Cardillo G, Viggiano G.V, et al. Fondaparinux use in patients with COVID-19: a preliminary multicenter real-world experience. *J Cardiovasc Pharmacol.* 2020;76:369-371.

87. Campos MA, Geraghty P, Holt G, et al. The biological effects of double-dose alpha-1 antitrypsin augmentation therapy a pilot clinical trial. *Am J Respir Crit Care Med.* 2019;200:318-326.
88. Van Norman GA, Gernsheimer T, Chandler WL, Cochran RP, Spiess BD. Indicators of fibrinolysis during cardiopulmonary bypass after exogenous antithrombin-III administration for acquired antithrombin III deficiency. *J Cardiothorac Vasc Anesth.* 1997;11:760-763.
89. Kanbak M. The treatment of heparin resistance with antithrombin III in cardiac surgery. *Can J Anaesth.* 1999;46:581-585.
90. Lemmer JH, Despotis GJ. Antithrombin III concentrate to treat heparin resistance in patients undergoing cardiac surgery. *J Thorac Cardiovasc Surg.* 2002;123:213-217.
91. Koster A, Chew D, Kuebler W, Habazettl H, Hetzer R, Kuppe H. High antithrombin III levels attenuate hemostatic activation and leukocyte activation during cardiopulmonary bypass. *J Thorac Cardiovasc Surg.* 2003;126:906-907.
92. Diaz R, Moffett BS, Karabinas S, Guffrey D, Mahoney DH Jr, Yee .L. Antithrombin concentrate use in children receiving unfractionated heparin for acute thrombosis. *J Pediatr.* 2015;167:645-649.
93. Ryerson LM, Bruce A.K, Lequier L, Kuhle S, Massicotte M.P, Bauman M.E. Administration of antithrombin concentrate in infants and children on extracorporeal life support improves anticoagulation efficacy. *ASAIO J.* 2014;60:559-563.
94. Rogenhofer N, Bohlmann M.K, Beuter-Winkler P, et al. Prevention, management and extent of adverse pregnancy outcomes in women with hereditary antithrombin deficiency. *Ann Hematol.* 2014;93:385-392.
95. Camprubi-Rimblas M, Tantinyà N, Guillamat-Prats R, et al. Effects of nebulized antithrombin and heparin on inflammatory and coagulation alterations in an acute lung injury model in rats. *J Thromb Haemostasis.* 2020;18:571-583.
96. Sun HM, Hong LZ, Shen XK, Lin XQ, Song Y, Shi Y. Antithrombin-III without concomitant heparin improves endotoxin-induced acute lung injury rats by inhibiting the activation of mitogen-activated protein kinase. *Chin Med J.* 2009;122:2466-2471.
97. Lippi G, Henry BM, Sanchis-Gomar F. Plasma antithrombin values are significantly decreased in coronavirus disease 2019 (COVID-19) patients with severe illness. *Semin Thromb Hemost.* 2021;47:460-462.

#### SUPPORTING INFORMATION

Additional supporting information can be found online in the Supporting Information section at the end of this article.

**How to cite this article:** Wettstein L, Immenschuh P, Weil T, et al. Native and activated antithrombin inhibits TMPRSS2 activity and SARS-CoV-2 infection. *J Med Virol.* 2022;1-13. doi:10.1002/jmv.28124